β-adrenergic control of sarcolemmal $Ca_V1.2$ abundance by small GTPase Rab proteins

Silvia G. del Villar, Taylor L. Voelker, Heather C. Spooner, Eamonn J. Dickson, and Rose E. Dixon*.

Dept. of Physiology and Membrane Biology, University of California, Davis, CA

*To whom correspondence should be addressed:
Rose E. Dixon
University of California, Davis
Department of Physiology & Membrane Biology
School of Medicine, Tupper Hall, room 4112
One Shields Avenue
Davis, California 95616

Phone: (530) 754-0742
Email: redickson@ucdavis.edu

https://orcid.org/0000-0002-5612-4761
https://orcid.org/0000-0002-6779-9350
https://orcid.org/0000-0002-0873-8021
https://orcid.org/0000-0001-8619-7630
https://orcid.org/0000-0003-0655-690X

Classification
BIOLOGICAL SCIENCES I Physiology

Keywords
L-type calcium channel I heart I β-adrenergic receptor I trafficking I clustering

Author Contributions
R.E.D. conceived experiments, R.E.D. and S.G.V. designed experiments, S.G.V., T.V., and H.C.S. executed experiments, S.G.V., T.V. and R.E.D. analyzed data and prepared figures, S.G.V. and R.E.D. wrote the paper, R.E.D. and E.J.D. interpreted data and all authors read and revised the manuscript.

This PDF file includes:
- Main Text
- Figures 1 to 7
- Tables 1
- SI Appendix

Abstract

The number and activity of $Ca_v1.2$ channels in the cardiomyocyte sarcolemma tunes the magnitude of Ca^{2+}-induced Ca^{2+} release and myocardial contraction. β-adrenergic receptor (*βAR*) activation stimulates sarcolemmal insertion of $Ca_V1.2$ channels. This supplements the pre-existing sarcolemmal $Ca_V1.2$ population, forming large 'super-clusters' wherein neighboring channels undergo enhanced cooperative-gating behavior, amplifying Ca^{2+} influx and myocardial contractility. Here, we determine this stimulated insertion is fueled by an internal reserve of early- and recycling endosome-localized, pre-synthesized $Ca_V1.2$ channels. *βAR*-activation decreased $Ca_V1.2$/endosome colocalization in ventricular myocytes, as it triggered 'emptying' of endosomal $Ca_V1.2$ cargo into the sarcolemma. We examined the rapid dynamics of this stimulated insertion process with live-myocyte imaging of channel trafficking, and discovered that $Ca_V1.2$ are often inserted into the sarcolemma as pre-formed, multi-channel clusters. Likewise, entire clusters were removed from the sarcolemma during endocytosis, while in other cases, a more incremental process suggested removal of individual channels. The amplitude of the stimulated insertion response was doubled by co-expression of constitutively-active Rab4a, halved by co-expression of dominant-negative Rab11a, and abolished by co-expression of dominant-negative mutant Rab4a. In ventricular myocytes, *βAR*-stimulated recycling of $Ca_V1.2$ was diminished by both nocodazole and latrunculin-A, suggesting an essential role of the cytoskeleton in this process. Functionally, cytoskeletal disruptors prevented *βAR*-activated Ca^{2+} current augmentation. Moreover, *βAR*-regulation of $Ca_V1.2$ was abolished when recycling was halted by co-application of nocodazole and latrunculin-A. These findings reveal that *βAR*-stimulation triggers an on-demand boost in sarcolemmal $Ca_V1.2$ abundance via targeted, Rab4a and Rab11a-dependent insertion of $Ca_V1.2$ channels is essential for *βAR*-regulation of cardiac $Ca_V1.2$.

Significance Statement

The L-type voltage-gated Ca^{2+} channel $Ca_V1.2$ is essential for excitation-contraction coupling in the heart. During the fight-or-flight response, $Ca_V1.2$ channel activity is augmented as a result of PKA-mediated phosphorylation, downstream of β-adrenergic receptor (*βAR*) activation. We discovered that enhanced sarcolemmal abundance of $Ca_V1.2$ channels, driven by stimulated insertion/recycling of specific $Ca_V1.2$ containing endosomes, is essential for *βAR*-mediated regulation of these channels in the heart. These data reveal a new conceptual framework of this critical and robust pathway for on-demand tuning of cardiac EC-coupling during fight-or-flight.

Main Text

Introduction

Ca^{2+} influx through L-type Ca^{2+} channels ($Ca_V1.2$) is indispensable for cardiac excitation-contraction coupling (EC-coupling) (1). These multimeric proteins consist of a pore-forming and voltage-sensing α_{1c} subunit, and auxiliary β and $\alpha_2\delta$-subunits. In ventricular myocytes, $Ca_V1.2$ mainly localize to the t-tubule sarcolemma and open briefly, allowing a small amount of Ca^{2+} influx, in response to the wave of depolarization that travels through the conduction system of the heart from its point of origin, usually in the SA-node. This initial influx is amplified manifold though Ca^{2+}-induced Ca^{2+} release (CICR) from juxtaposed type 2 ryanodine receptors (RyR2) on the junctional sarcoplasmic reticulum (jSR), Which are localized a short ~12 nm across the dyadic cleft. The synchronous opening of thousands of RyR2 generates a transient, global elevation in intracellular calcium concentration ($[Ca^{2+}]_i$), resulting in contraction. Reducing $Ca_V1.2$ channel current (I_{Ca}) results in less CICR, smaller $[Ca^{2+}]_i$ transients, and less forceful contractions. Conversely, larger amplitude I_{Ca} elicits greater Ca^{2+} release from the SR, producing more forceful contractions. The level of Ca^{2+} influx through $Ca_V1.2$ channels therefore tunes EC-coupling.

I_{Ca} is a product of the number of channels in the sarcolemma and their open probability (P_o). Consequently, there are two possible, non-mutually exclusive strategies that may be adopted to alter I_{Ca} and consequently the magnitude of EC-coupling: i) adjust $Ca_V1.2$ channel activity (P_o) and/or, ii) modify sarcolemmal $Ca_V1.2$ channel expression (N). The first strategy of increasing channel P_o has long been associated with β-adrenergic receptor (*βAR*)-mediated signaling in the heart (2-4). During acute physical or emotional stress, norepinephrine spills from sympathetic varicosities onto cardiomyocytes, activating *βAR*s. The ensuing $G_{\alpha s}$/adenylyl cyclase/cAMP/PKA signaling cascade culminates in PKA phosphorylation of several effector proteins, including $Ca_V1.2$ (or an element of their interactome (5, 6)), enhancing their activity to generate this positive inotropic response.

As to the second strategy to increase I_{Ca}, there remains a paucity of information regarding the mechanisms regulating $Ca_V1.2$ channel abundance in the cardiomyocyte sarcolemma. Classical secretory transport literature suggests that $Ca_V1.2$ channels are trafficked from

the endoplasmic reticulum (ER) to the trans-Golgi-network (TGN) and onward to their dyadic position in the sarcolemma. Underscoring the importance of faithful $Ca_V1.2$ channel trafficking, altered $Ca_V1.2$ channel density has been reported in both failing (7, 8) and aging (9) ventricular myocytes, and impaired anterograde trafficking of $Ca_V1.2$ channels to the t-tubules of human ventricular myocytes has been linked to dilated cardiomyopathy (10). Yet, despite the importance of tight homeostatic control of $Ca_V1.2$ channel trafficking to prevent Ca^{2+} dysregulation, the molecular steps defining $Ca_V1.2$ channel sorting and insertion remain poorly understood. Therefore, elucidation of the trafficking pathways that regulate $Ca_V1.2$ channel abundance is critical for our understanding of the pathophysiology of heart failure and myocardial aging, and could potentially reveal new therapeutic or rejuvenation targets. Along that vein, in the treatment of cystic fibrosis, multiple drugs are in various stages of use or development to improve trafficking to, or to amplify, or stabilize, CFTR channels at the apical membrane of airway epithelial cells (11).

There have been no measurements of $Ca_V1.2$ channel lifetimes in cardiomyocytes, but pulse-chase experiments in immortalized cell lines support a lifetime of plasma membrane (PM)-localized $Ca_V1.2$ channels of ~3 h (12) while total cellular $Ca_V1.2$ lifetime is >20 h (13, 14). This disparity suggests membrane-$Ca_V1.2$ turns over much more dynamically than the total cellular channel content and implies ongoing local control by endosomal trafficking. Disturbance of the equilibrium between channel insertion/recycling and internalization would be predicted to lead to alterations in sarcolemmal $Ca_V1.2$ channel abundance. Trafficking of vesicular cargo through the endosomal pathway is regulated by Rab-GTPases, a >60-member family within the larger Ras superfamily of small GTPases (15-18). Rab5 is involved in endocytosis and control of vesicular cargo influx into early endosomes (EEs; also called sorting endosomes), while Rab4 controls efflux of cargo out of EEs and fast recycling ($t_{1/2}$ ~1-2 min) back to the PM (19). Rab11, expressed on recycling endosomes (RE; also called the endocytic recycling compartment or ERC), regulates slow recycling ($t_{1/2}$ ~12 min) of cargo from this compartment back to the PM (19). In cortical neurons and pancreatic β-cells, activity-dependent $Ca_V1.2$ channel internalization has been postulated to play important roles in Ca^{2+} homeostasis, with implications for homeostatic synaptic plasticity and insulin production respectively (20). In mouse neonatal cardiomyocytes, Rab11b has been reported to limit expression PM $Ca_V1.2$ (21), while recent studies performed in HEK and HL-1 cells reported that endocytic

recycling of cardiac $Ca_V1.2$ channels, regulates their surface abundance (13, 22). Despite this crucial information from other cell-types, there has been a lack of rigorous investigations, at the molecular level, into how $Ca_V1.2$ channel recycling is regulated in cardiac myocytes.

Here, we identify a dynamic, sub-sarcolemmal pool of $Ca_V1.2$-cargo-carrying endosomes that are rapidly mobilized to the ventricular myocyte sarcolemma along targeted Rab4a and Rab11a GTPase-regulated recycling pathways in response to βAR-stimulation. Using electrophysiology, cell biology approaches, TIRF and super-resolution microscopy, we report that enhanced sarcolemmal $Ca_V1.2$ abundance via targeted, ISO-stimulated, recycling of $Ca_V1.2$ channels is essential for *β*AR-regulation of cardiac $Ca_V1.2$.

Results

Internal pools of pre-synthesized $Ca_V1.2$ channels reside on endosomes

Recently, we reported that sarcolemmal $Ca_V1.2$ channel expression increases in the heart during *βAR* signaling (23). Activation of *βAR*s with isoproterenol (ISO) produced a rapid, PKA-dependent augmentation of $Ca_V1.2$ channel abundance along ventricular myocyte t-tubules. We hypothesized that an endosomal pool of $Ca_V1.2$ fuels the rapid, ISO-stimulated insertion of channels into the sarcolemma of ventricular myocytes. To test this, we performed an examination of the distribution of $Ca_V1.2$ channels on EEs, REs and late endosomes (LEs) in adult mouse ventricular myocytes (AMVMs) using two- or three-color Airyscan super-resolution microscopy. Immuno-stained $Ca_V1.2$ channel cargo was observed on 15.1 ± 0.4 % of early endosome antigen-1 (EEA1) positive pixels in male ventricular myocytes and on a similar 16.1 ± 0.7 % in female myocytes (Figure 1A and B; $P = 0.24$; see also Figure S1). Pre-fixation stimulation with 100 nM ISO led to a significant, 15-20 % decrease in colocalization between $Ca_V1.2$ and EEA1 (male $P = 0.001$, female $P = 0.01$). We further narrowed our analysis to Rab4 positive EEs by performing triple-label experiments, co-staining for $Ca_V1.2$, EEA1, and Rab4 (Figure S2). A similar trend was observed there such that 15.6 ± 1.3 % of EEA1- and Rab4 co-expressing pixels were colocalized with $Ca_V1.2$, falling to 10.8 ± 0.6 % in ISO-stimulated cells ($P = 0.008$). These data suggest that ISO activation of *βAR*s, stimulates movement of $Ca_V1.2$ out of EEs and into another cellular compartment.

Cargo exiting the EE can be routed either to REs, LEs, or back to the sarcolemma via the fast recycling pathway (see working model in Figure 7A) (17, 19). If *βAR* activation stimulates $Ca_V1.2$ channel trafficking from EEs into REs then a testable prediction is that ISO should increase colocalization between $Ca_V1.2$ and Rab11 (a marker of REs). Accordingly, we examined the distribution of $Ca_V1.2$ on Rab11-positive REs, and found a population of $Ca_V1.2$-cargo-carrying REs, where $Ca_V1.2$ colocalized with 14.9 ± 0.5 % of Rab11-positive pixels in males and with 13.3 ± 0.6 % in females (Figure 1C and D). An 18% decrease in colocalization between $Ca_V1.2$ and Rab11 was observed in male cells treated with 100 nM ISO ($P = 0.002$). Data from female cardiomyocytes showed a similar downward trend in colocalization. These results do not support the hypothesis that $Ca_V1.2$ channels move from Rab4-positive EEs into REs in response to ISO. We next tested the

hypothesis that ISO stimulation drives the trafficking of $Ca_V1.2$ channels from EEs to LEs, however despite identifying a population of $Ca_V1.2$ channels on Rab7-positive LEs in male and female ventricular myocytes, ISO stimulation did not significantly alter the degree of Rab7/$Ca_V1.2$ colocalization (Figure 1E and F; $P = 0.28$ in males, $P = 0.39$ in females). Having ruled out two of the three possibilities, we surmise that βAR stimulation drives an intracellular pool of $Ca_V1.2$ channels from Rab4-positive EEs into the fast recycling pathway, and Rab11-positive REs into the slow recycling pathway.

ISO-stimulated enhancement of $Ca_V1.2$ recycling is regulated by Rab4 and Rab11

Having determined that *βAR* stimulation decreases the number of $Ca_V1.2$ channels on EEs and REs we next tested if Rab4-dependent fast and, Rab11-dependent slow recycling pathways facilitate enhancement of $Ca_V1.2$ delivery into the PM of transiently transfected tsA201 cells. While these cells do not recapitulate all of the intricacies of signaling in cardiomyocytes, we utilized them here because, 1) they provide a reductionist framework on which to test our Rab4 and Rab11 hypotheses in the absence of other voltage-gated channels; 2) they can be easily transfected, permitting manipulation of Rab-protein complement; and 3) they endogenously express *βARs* (24). PM expression of $Ca_V1.2$ channels was monitored during activation of *βARs* with 100 nM ISO. Clusters of channels were readily identified in the TIRF footprint of the cell (Figure 2A). Upon wash-in of ISO, $Ca_V1.2$-tagRFP intensity in the TIRF footprint increased by an average of 1.37-fold over a period of minutes (Figure 2B; τ_{on} = 2.26 ± 0.02 min), in close agreement with previous results showing a 44.9 ± 6.2 % increase in channels in ISO-stimulated AMVM sarcolemmas (23). An increased density (number/μm^2) of channel clusters in the TIRF footprint contributed to this elevation (Figure 2C; $P < 0.0001$). These results suggest that ISO stimulates enhanced recycling of $Ca_V1.2$ channels to the PM.

We tested the role of Rab4a in this dynamic response by co-expressing a mutant Rab4a with a single amino acid substitution (Q67L) that renders it resistant to GTP-hydrolysis, locking it in a GTP-bound, constitutively active state (CA-Rab4a^{Q67L}; Figure 2D-F) (25). In these cells, addition of ISO stimulated a 1.69-fold increase in intensity, almost twice the maximal response observed in controls, and increased cluster density 2.4-fold (Figure 2F; $P = 0.002$). Interestingly, co-expression of CA-Rab4a had no effect on basal $Ca_V1.2$ cluster density before addition of ISO ($P = 0.08$; Figure 2C and F) indicating that even in this GTP-

locked active state, ISO-stimulation is required to trigger the boost in $Ca_V1.2$ recycling. After ISO, the GTP-bound CA-Rab4a facilitates a larger, faster (1.76 ± 0.02 min) recycling response. This suggests that Rab4a plays a role in *β*AR-stimulated channel recycling but also implies the involvement of an upstream effector.

To support this postulate, we examined the ISO response in cells expressing a dominant-negative, GDP-locked variant of Rab4 (DN-Rab4^{S22N}). Under these conditions, ISO-application failed to enhance $Ca_V1.2$ surface expression and instead a slight decrease in $Ca_V1.2$-tagRFP intensity and cluster density was observed in the PM over the course of the experiment (Figure 2G, H, and I). These results confirm that Rab4a is part of the essential trafficking machinery that underlies the ISO-stimulated enhanced recycling of $Ca_V1.2$.

Since a subpopulation of $Ca_V1.2$ channels that localize to Rab11 positive REs was also identified in AMVMs (Figure 1C and D) , we tested the role of Rab11a in this dynamic recycling response to ISO using a dominant negative, GDP-locked DN-Rab11a^{S25N}. Despite impaired Rab11a function, an ISO-stimulated increase in $Ca_V1.2$-tagRFP intensity was still evident, albeit to a lesser extent than in controls (1.12-fold; Figure 2J and K). This was accompanied by a 1.49-fold increase in cluster density (P = 0.009; Figure 2L). Accordingly, DN-Rab11a-mediated knock down of Rab11a activity generated ~33% of the response seen in controls while knock down of Rab4a abolished the response (Figure 2H and M). These data suggest that upstream Rab4a activity is necessary, not only for fast recycling to the PM but also for transfer of $Ca_V1.2$ cargo from EEs to REs. Impaired Rab4a function creates a 'road block' in the endosomal recycling system. The role of Rab4a in fast recycling was unmasked in cells with knocked down Rab11a activity, where τ_{on} of the stimulated recycling response was 0.96 ± 0.02 min (Figure 2K), significantly faster than controls where both Rab4a and Rab11a were active (2.26 ± 0.02 min). A theoretical time course of the slow Rab11a-dependent contribution was calculated by subtracting the predominantly Rab4a-mediated recycling time-course in DN-Rab11a expressing cells from endogenous Rab controls (Figure 2M). This theoretical Rab11a-dependent response displayed a 1.29-fold increase in $Ca_V1.2$-tagRFP intensity and was well-fit with a single exponential function with a τ_{on} = 2.69 ± 0.04 min that was slower than control or Rab4a-mediated responses. Based on these data, our results suggest that $Ca_V1.2$ channels

stimulated to recycle to the PM in response to *βAR* activation are sourced approximately 1/3rd from the fast Rab4a, and 2/3rd from the slow Rab11a recycling pathways.

Actin and microtubule disruption impairs ISO-stimulated $Ca_V1.2$ recycling

We used Airyscan super-resolution microscopy to examine $Ca_V1.2$ channel proximity to microtubules (MTs) and actin filaments (Figure 3A-B). Immunostaining with α-tubulin revealed the extensive MT cytoskeleton with its lattice, grid-like appearance in the subsarcolemma, transitioning to a more longitudinally-oriented network deeper in the cell interior (Figure 3A). $Ca_V1.2$ channels decorate the MTs in both locations. Phalloidin-staining of the actin network revealed the periodic alignment of sarcomeric actin (Figure 3B). It is notoriously difficult to visualize cortical actin in cardiomyocytes due to the overwhelming abundance of sarcomeric actin but in many locations $Ca_V1.2$ channels were co-localized with actin (Figure 3B, white arrowheads). The degree of colocalization between $Ca_V1.2$ and, in particular MTs, implies a role for the cytoskeleton in regulating channel availability.

To study the role of these cytoskeletal highways in *βAR*-stimulated $Ca_V1.2$ mobilization from endosomes, we examined EEA1-localized $Ca_V1.2$ channel populations in AMVMs treated with cytoskeletal disruptors. Accordingly, freshly isolated myocytes were treated for 2 hrs with 10 μM nocodazole, a drug known to prevent addition of tubulin to dynamic MTs, and depolymerize the stable variety (26). Immuno-staining with anti-α-tubulin confirmed the treatment had substantially disordered the MTs (Figure 3C). In this and upcoming experimental series, we refer to cells that did not receive cytoskeletal disruptors as 'untreated'. As in untreated cells (Figure 1A and B), $Ca_V1.2$ was observed to colocalize with a sub-population of EEs (16.9 ± 0.6 %; Figure 3D and E). However, in cells stimulated with 100 nM ISO prior to fixation, the reduction in colocalization between EEA1 and $Ca_V1.2$ we had previously observed in untreated cells was absent in nocodazole-treated cells, instead remaining at 17.5 ± 0.7 % (P = 0.51 compared to nocodazole-treated control). These data suggest that MT network disruption prevents the 'emptying' of $Ca_V1.2$ channel cargo from the EEs into the sarcolemma and support a role for MTs and their associated motor proteins as conduits for ISO-stimulated $Ca_V1.2$ recycling.

We then examined the role of the actin cytoskeleton by disrupting it with latrunculin A (lat-A; 5 μM for 2 hrs), which both facilitates F-actin depolymerization (27) and prevents polymerization by sequestering actin monomers (26). Importantly, lat-A specifically affects the actin cytoskeleton but spares the MT network (28). Alexa Fluor 647-conjugated phalloidin staining of filamentous-actin (F-actin) was used to visually confirm lat-A mediated actin-disruption (Figure 3F). In lat-A-treated myocytes, $Ca_V1.2$ and EEA1 colocalization was similar to untreated controls (16.2 ± 0.7 % versus 15.1 ± 0.4 %; P = 0.14). However, ISO-stimulation did not affect colocalization levels (16.7 ± 0.5 %; P = 0.64; Figure 3G and H). In addition, in cells co-treated with nocodazole and lat-A, ISO-stimulation actually promoted a small, but significant increase in colocalization between $Ca_V1.2$ and EEA1 (P = 0.03; Figure 3I and J). These data indicate a profound alteration in the endosomal pathway where recycling and or endocytosis have been impaired, creating an 'endosomal traffic jam' leading to accumulation of cargo on the endosomes, with no cytoskeletal highways to transport the cargo to its destination.

Cytoskeletal disruption alters ISO-stimulated $Ca_V1.2$ dynamics and recycling

Real-time visualization and quantification of the effects of cytoskeletal disruption on channel trafficking was performed using transduced AMVMs isolated from mice that had received a retro-orbital injection of AAV9-$Ca_V\beta_{2a}$-paGFP. This auxiliary subunit of $Ca_V1.2$ binds to the pore-forming subunit with a 1:1 stoichiometry and acts in this context as a biosensor reporting the location of the subset of $Ca_V1.2$ α_{1c} it interacts with. This approach was previously validated by our group (23), with super-resolution microscopy experiments confirming that the biosensor and the α_{1c} colocalize, and unlike overexpression of α_{1c}, at these concentrations we have found that $Ca_V\beta_{2a}$-paGFP transduction does not appreciably affect $Ca_V1.2$ α_{1c} expression as indicated by unaltered basal channel cluster sizes. A further advantage of this approach is that it requires no culturing of AMVMs which are known to rapidly dedifferentiate in culture (29). We began by examining the dynamic channel trafficking response to ISO in untreated AMVMs (i.e., in the absence of cytoskeletal disruptors) using TIRF microscopy. Discrete puncta of $Ca_V\beta_{2a}$-paGFP decorated the TIRF footprint of the myocyte during control frames and additional puncta/clusters were seen to appear in the TIRF footprint supplementing the initial complement after perfusion with 100 nM ISO (Movie 1 and Figure 4A). Given our

endosome/$Ca_V1.2$ immunostaining results (Figure 1), this may represent endosomal cargo mobilized in response to ISO from subsarcolemmal locations deeper within the cell. In agreement with this, 3D-plots of $Ca_V\beta_{2a}$-paGFP intensity over time and cell depth, constructed from 4D-spinning disk confocal experiments performed on transduced AMVMs at 37°C, indicated $Ca_V\beta_{2a}$-paGFP was mobilized from several microns within the cell, and moved toward the surface in response to ISO (Figure S3). At physiological temperature, following a delay of ~3 sec, the response to ISO proceeded monoexponentially with a $\tau = 2.53 \pm 0.28$ sec until $Ca_V\beta_{2a}$-paGFP intensity reached a plateau (Figure S3C-D), presumably achieved when the endosomal pool of channels had been depleted and balance between insertion and endocytosis reached a new equilibrium. These data fit well with previous measurements of the time course of I_{Ca} responses to ISO (30, 31). Interestingly, exchange of the perfusate with one containing 100 nM of angiotensin II, quickly reversed the response, and a subset of $Ca_V\beta_{2a}$-paGFP moved back into the interior of the cell with a $\tau = 2.94 \pm 0.96$ sec. Previous work performed at room temperature reported that prolonged (30 - 60 min) application of angiotensin II produces $Ca_V1.2$ channel internalization (32), but here at physiological temperature, the time course was significantly accelerated.

To test the hypotheses that ISO treatment increases sarcolemmal expression of $Ca_V1.2$ by stimulating channel insertion/recycling, and that cytoskeletal highways carry these recycling channels to their destination, we performed 'image math' (see Methods) on TIRF time series to quantify the subpopulations of $Ca_V\beta_{2a}$-paGFP in the TIRF-footprint that were: i) inserted, ii) endocytosed, and iii) stably expressed during ISO stimulation. Responses to ISO in untreated AMVMs were compared, to those in cells treated with nocodazole, lat-A, or a combination of both (Figure 4). Live cell time series experiments revealed a dynamic population of $Ca_V\beta_{2a}$-paGFP in all cells examined (see Movies 1-4), although the dynamics were appreciably less in cells that received cytoskeletal disrupting treatments, supporting the idea that both F-actin and MTs are important conduits of this response. The number of channels at the sarcolemma at any given time, is dictated by the balance between channel insertions via the biosynthetic delivery and endosomal recycling pathways, and channel removals via endocytosis. In untreated cells, ISO stimulation heavily shifted the balance in favor of insertion, implying a stimulated insertion/recycling

process (Figure 4A, and E-G). This mismatch between insertion and endocytosis produced a 27.95 ± 4.31 % increase in sarcolemmal $Ca_V\beta_{2a}$-paGFP expression (Figure 4E). The time course of ISO-stimulated insertions of channels in untreated AMVMs can be observed in the ROIs highlighted in Figure 4A. Examination of these time courses revealed rapid step-like insertion profiles, suggesting that $Ca_V1.2$ appear to often insert into the sarcolemma as preformed clusters, containing many channels (Figure 4A(i-iii), B(ii and iii), C(ii and iii), D(i and ii)). In some cases, a delivery hub was evident, where a succession of channel clusters appeared to insert one after the other (Figure 4A(ii) and B(iii)). Channel endocytosis also appeared to involve removal of channel clusters in some instances (Figure 4C(i), D(iii)), while in other ROIs, a slower, gradual removal of potentially individual channels was more evident (Figure 4B(i)).

Recycling of endosomal cargo back to the PM is known to rely on both MTs and actin (33). Indeed, cytoskeletal disruption reduced the magnitude of the ISO-stimulated augmentation of sarcolemmal $Ca_V\beta_{2a}$-paGFP expression compared to untreated cells (Figure 4E). Interestingly, how the two elements of the cytoskeleton affected the ISO-stimulated change in sarcolemmal expression varied somewhat, as revealed by examination of insertion and endocytosis events in each AMVM cohort. Anterograde transport and targeting of $Ca_V1.2$ to the t-tubule membrane is known to occur along MTs, anchored there via the BAR-domain containing protein, BIN1 (A.K.A. amphiphysin II) (34). Here, our experiments were focused not on long distance trafficking from the trans-golgi to the membrane, but rather from the local endosome pool of channels and thus channel dynamics were observed over short 3 min periods before and after application of ISO. Our data indicates that nocodazole mediated MT disruption reduced ISO-stimulated insertion of $Ca_V\beta_{2a}$-paGFP by an average of ~70% compared to untreated cells (Figure 4F). Channel internalization and the lifetime of channels in the membrane was not affected by the degree of MT disruption tested here, as both endocytosed and static channel population sizes were not significantly altered by this treatment (Figure 4G and H).

Actin disruption with lat-A in contrast had no significant effect on channel insertion compared to untreated cells (Figure 4F). In neurons and HEK293 cells, interactions between $Ca_V1.2$ and the actin-interacting protein α-actinin have been found to stabilize $Ca_V1.2$ channel expression at the PM (35, 36). A notable trend toward increased

endocytosis of $Ca_V\beta_{2a}$-paGFP in lat-A treated cells was detected but this failed to reach significance assessed by a one-way ANOVA test (Figure 4G). There was also a trending increase in the fraction of stable $Ca_V\beta_{2a}$-paGFP in the TIRF footprint that appeared to be left 'stranded' there (Figure 4H), perhaps reflective of incomplete internalization of $Ca_V\beta_{2a}$-paGFP due to the lack of actin dynamics and the disrupted cortical actin network. This effect was not statistically different from controls but was significantly different from nocodazole treated cells. Finally, combined treatment with nocodazole and lat-A actually *reduced* the overall expression of $Ca_V\beta_{2a}$-paGFP in the TIRF footprint by 8.63 ± 6.76 % over the course of the experiment (Figure 4F and G). This occurred when the balance of endocytosis and insertion/recycling shifted in favor of endocytosis. Collectively, these data suggest that MTs and actin are both important conduits of *βAR*-stimulated $Ca_V1.2$ recycling, with MTs playing the major role in channel insertion.

βAR mediated I_{Ca} regulation is abrogated by cytoskeletal disruption

To ascertain whether ISO-stimulated recycling of $Ca_V1.2$ channels into the cardiomyocyte sarcolemma makes any functional contribution to the *βAR* regulation of these channels, we performed whole cell patch clamp recordings on freshly isolated AMVMs under various cytoskeletal disrupting conditions. Stimulation of untreated cardiomyocytes with 100 nM ISO, produced a significant 1.65 ± 0.19-fold enhancement of I_{Ca} ($P = 0.04$; Figure 5A and B) and caused a 13.33 ± 1.49 mV leftward-shift in the voltage-dependence of conductance (measured as the difference between $V_{1/2}$ of each fit; $P < 0.0001$; Figure 5C and Table 1). In addition, we observed an increase in the slope steepness of the Boltzmann function used to fit the G/G_{max} data from 5.45 ± 0.84 in controls to 4.90 ± 1.06 in 100 nM ISO (Figure 5C and Table 1), suggesting a potential increase in cooperative gating behavior (23).

The impact of MT disruption on the I_{Ca} response to ISO was tested in AMVMs incubated with nocodazole. This dose and duration of treatment did not alter control I_{Ca} amplitude (compared to untreated control). Indeed, none of the cytoskeletal disrupting treatments had any significant effect on control I_{Ca} with all of them peaking between -3.78 and -4.07 pA/pF (Figure 5B, E, H, and K). However, nocodazole blunted the I_{Ca} response to ISO by ~72% (1.18 ± 0.08-fold increase versus 1.65-fold change in untreated cells), halved the magnitude of leftward-shift of the voltage dependence of conductance (6.73 ± 1.38 mV

versus the 13.33 mV shift in untreated cells), and eliminated the tendency toward cooperativity indicated by the slope of the Boltzmann function used to fit the G/G_{max} (Figure 5D-F; Table 1).

We used the same experimental paradigm to test whether the actin cytoskeleton plays any role in the functional regulation of $Ca_V1.2$ by *βAR*s. Cells treated with lat-A exhibited a 40% reduction in the I_{Ca} augmentation response to ISO compared to controls (Figure 4G and H, Table 1), and a similar halving of the leftward-shift in the voltage dependence of conductance as in nocodazole-treated cells (5.92 ± 1.63 shift; Figure 5I and Table 1). ISO stimulation produced G/G_{max} data that was well-fit with a Boltzmann function that was less steep than in ISO-stimulated untreated cells but still indicated enhanced cooperativity (Figure 5I and Table 1).

Finally, we examined the effect of ISO on I_{Ca} when both MTs and actin filaments were disrupted with a combined nocodazole and lat-A treatment. Under these conditions, *βAR*-mediated regulation of $Ca_V1.2$ was essentially abolished (Figure 5J-K), with ISO, generating only a 1.01 ± 0.11-fold increase in I_{Ca}, representing a 98% reduction in the response compared to untreated cells. The leftward-shift in the voltage dependence of conductance was reduced to 2.54 ± 1.49, equivalent to only 20% of the response seen in untreated cells. The slope factor of the Boltzmann-function used to fit the data was less steep than untreated cells in both control and ISO-stimulated conditions, indicating reduced cooperativity. These functional data collectively indicate that an intact cytoskeleton is an essential requirement for *βAR*-mediated regulation of $Ca_V1.2$.

Clustering of $Ca_V1.2$ channels is supported by the cytoskeleton

The observation that channel cooperativity was altered in AMVMs with disrupted cytoskeletal elements implies that the cytoskeleton might be important not only for *βAR*-mediated regulation of $Ca_V1.2$ but also for the stabilization and support of channel clusters. We tested this idea by examining $Ca_V1.2$ channel distribution with Ground State Depletion (GSD) super-resolution nanoscopy. ISO-stimulation resulted in the formation of $Ca_V1.2$ channel super-clusters in AMVMs which were, on average, 22.6% larger than the clusters in control AMVMs (Figure 6A and E). Super-clustering could occur due to small clusters

fusing together to form larger ones, or alternatively, could reflect enhanced sarcolemmal expression of $Ca_V1.2$. If the superclusters form because of enhanced insertion/exocytosis of $Ca_V1.2$ into the sarcolemma, then a testable prediction is that the intensity of the fluorescence emission (normalized to the cell area) should be increased. In contrast, if the super-clusters simply reflect fusion of existing sarcolemmal $Ca_V1.2$ clusters then the total fluorescence intensity should be similar in control and ISO-treated cells. Accordingly, the normalized total integrated density was significantly larger in ISO-treated cells than controls (Figure 6F; P = 0.00002), in agreement with the idea that *βAR*-activation stimulates enhanced sarcolemmal insertion and resultant super-clustering of $Ca_V1.2$ channels. Cytoskeletal disruption with nocodazole (Figure 6B), lat-A (Figure 6C), or a combination of the two (Figure 6D), did not affect basal channel expression in the sarcolemma as indicated by similar cluster areas and total integrated density values (Figure 6E-F). These results validate the unaltered I_{Ca} observed in unstimulated cells from each of our four experimental groups (Figure 5) and supports the postulate that the lifetime of these channels in the membrane is longer than the 2 h cytoskeletal disruption period. In addition, ISO-stimulation failed to induce super-clustering or enhanced sarcolemmal expression of $Ca_V1.2$ in AMVMs (Figure 6E-F). Altogether, these data suggest that both intact MTs and actin are necessary for the formation of $Ca_V1.2$ super clusters in response to ISO stimulation.

Discussion

The data presented in the present study provide the first report of an endosomal pool of $Ca_V1.2$ channels in cardiomyocytes that undergoes rapid, targeted mobilization to the sarcolemma in response to *βAR*-activation, effectively creating an 'on-demand' trafficking pathway to facilitate a positive inotropic response during fight-or-flight. We present six major new findings: 1) intracellular pools of $Ca_V1.2$ channels are present on EEs, REs, and in LEs and lysosomes in AMVMs; 2) *βAR*-activation triggers $Ca_V1.2$ mobilization from EEs and REs to the sarcolemma via Rab4a-dependent fast, and Rab11a-dependent slow recycling pathways; 3) $Ca_V1.2$ are often inserted or removed from the sarcolemma as large multi-channel clusters, rather than individual channels; 4) stimulated insertion of $Ca_V1.2$ channels occurs along MTs; 5) the endosomal pool of $Ca_V1.2$ is fueled by actin-dependent endocytosis; and finally, 6) adrenergic regulation of $Ca_V1.2$ is abrogated by cytoskeletal disruption and loss of this dynamic recycling response. On the basis of these data, we present a new working model (Figure 7) for *βAR*-regulation of cardiac $Ca_V1.2$ channels in which stimulated recycling of $Ca_V1.2$, from sub-sarcolemmal pools of Rab4a and Rab11a-positive endosomes, results in enhanced expression of $Ca_V1.2$ at the membrane of AMVMs. Resultant super-clustering and cooperative gating of $Ca_V1.2$ channels contributes to the enhanced I_{Ca} and inotropic response.

Our data revealed pools of intracellular $Ca_V1.2$ channels on EEA1 and Rab4-positive EEs, on Rab11 positive REs, and in Rab7 positive LEs and lysosomes. In response to ISO, EE and RE-localized channels underwent rapid recycling into the sarcolemma via the Rab4a-dependent fast recycling pathway and the slower, Rab11a recycling pathway. While this is the first report of stimulated recycling of a recruitable intracellular reservoir of $Ca_V1.2$ in cardiomyocytes, small GTPase choreographed-recycling of endosome-localized ion channel pools are well-known to play a role in fine-tuning cellular responses to various stimuli including *βAR* stimulation. For example, in neurons, intracellular AMPA receptors (AMPAR) located on REs undergo Rab11-dependent recycling to the PM of dendritic spines in response to PKA-mediated phosphorylation of their GluA1 subunit at S845 downstream of β_2*AR* stimulation (reviewed in (37, 38)). In the collecting ducts of the kidney, vasopressin release initiates a G_s-coupled signaling cascade that triggers PKA-mediated phosphorylation of aquaporin-2 (AQP2) at S256 and consequent recycling of

AQP2 from Rab11-positive REs to the apical PM (39, 40). In the heart, acute stress initiates Rab11-dependent mobilization of endosomal reservoirs of SUR2-containing K_{ATP} channels and of KCNQ1-containing REs to the sarcolemma (41-44). Similarly, here we report an endosomal pool of $Ca_V1.2$ channels that undergoes 'on-demand', stimulated recycling upon activation of *βAR*s, providing a functional reserve that drives ventricular inotropy during sympathetic stimulation.

Despite their fundamental importance in cardiac EC-coupling, the difficulty in visualizing and measuring $Ca_V1.2$ channel dynamics means there is a remarkable lack of information about $Ca_V1.2$ channel trafficking, endocytosis, and recycling in cardiomyocytes, with much of the published data focusing instead on data collected from heterologous expression systems. A previous study found that shRNA knockdown of Rab11a did not affect Ba^{2+} currents through $Ca_V1.2$ in HEK293 cells or neonatal mouse ventricular myocytes while Rab11b knockdown significantly increased I_{Ba} (21), suggesting that Rab11b plays a contrary role to its close family member Rab11a, and actually regulates constitutive $Ca_V1.2$ channel degradation. While we did not measure currents from tsA201 cells, it is reasonable to expect that currents should scale proportionally with the number of $Ca_V1.2$ channels in the membrane, since the whole cell current (I_{Ca}) is the product of the number of channels (N), open probability (P_o), and single-channel current (i_{Ca}), i.e., $I_{Ca} = N \cdot i_{Ca} \cdot P_o$. We found no evidence that knockdown of Rab11a function affected basal channel cluster density (P = 0.12) or number of channels in the membrane (measured with normalized mean grey values; P = 0.16) (compared to same-day controls with no Rab overexpression), in agreement with the findings of Kamp et al. However, knockdown of Rab11a function reduced the degree of *βAR*-stimulated $Ca_V1.2$ insertion by 67%. This confirms the role of Rab11a in *βAR*-stimulated channel insertion rather than degradation.

Our work on live, AAV9-$Ca_V\beta_{2a}$-transduced AMVMs provides intriguing new insights into $Ca_V1.2$ channel trafficking, and captures the complex dynamics of these channels. We find that these channels are often inserted into the sarcolemma as entire pre-formed clusters at nucleation sites. Sometimes, repetitive insertions were seen to occur at an individual site, conjuring an image of $Ca_V1.2$-carrying endosomes queued up along MTs, anchored at a sarcolemmal delivery hub. Furthermore, channel endocytosis often appeared to occur via removal of entire clusters, while in other cases, a slower, gradual

removal of channels suggested ongoing removal of individual channels. Our results at physiological temperature indicate that these insertion and removal events occur extremely rapidly and can be stimulated by activation of GPCR-signaling pathways. Activation of *βAR*s was observed to increase the probability of channel insertion while activation of AngII receptors increased the probability of channel removal. These very scenarios were predicted in a recently published computer model designed to test the hypothesis that ion channel clustering occurs via a stochastic self-assembly process (45). Our data provides answers to the hypotheticals raised by that model. Informing that models parameters with the experimental data acquired in this study would be an interesting sequel.

One well-characterized facet of cardiac $Ca_V1.2$ channel trafficking is their targeted anterograde-delivery to the t-tubule membrane along BIN1-anchored MTs via the biosynthetic delivery pathway (34). Reduced levels of BIN1 in cardiomyocytes isolated from failing human hearts are associated with impaired $Ca_V1.2$ channel delivery and slower onset calcium transients (10). Here, we find that $Ca_V1.2$ channel recycling also occurs along MTs. Three independent lines of evidence support this conclusion. Firstly, MT disruption prevented ISO-stimulated mobilization of $Ca_V1.2$ from EE pools (Figure 3D). Secondly, MT disruption significantly reduced stimulated channel insertions in AAV9-$Ca_V\beta_{2a}$-paGFP transduced AMVMs (Figure 4F and Movie 2). Thirdly, ISO-stimulated $Ca_V1.2$ super-clustering was absent in nocodazole-treated AMVMs (Figure 6B and E). Our findings that basal $Ca_V1.2$ channel distribution and I_{Ca} amplitude were unaffected by 2 hr nocodazole treatment suggests that channel lifetime in the membrane is longer than 2 hrs, so that channels delivered along intact MTs prior to depolymerization by the drug, still largely remained there (Figure 6B). This agrees with previous measurements of PM $Ca_V1.2$ channel half-times of ~3 hrs, although this has never been directly measured in cardiomyocytes (12). However, despite negligible effects on basal channel expression and function, inhibition of MT polymerization significantly reduced ISO-stimulated responses, blunting I_{Ca} augmentation, and eliminating enhanced channel recycling and resultant super-clustering. Reduced MT polymerization occurs in human heart failure where stabilized MTs form a dense network in cardiomyocytes (46, 47). The lack of polymerization and potentially enhanced MT catastrophe rates, can result in traffic jams along MTs, leading to defective cargo delivery (46). Indeed, a previous study on live

ventricular myocytes reported reduced delivery of $K_V4.2$ and $K_V4.3$ channels to the sarcolemma due to increased MT catastrophe rates upon addition of hydrogen peroxide or in the ROS-rich post-myocardial infarction environment (48). Failing and aging myocytes display reduced $Ca_V1.2$ responsivity to ISO (49, 50), thus future studies should examine whether loss of adrenergic responsivity of $Ca_V1.2$ in HF occurs due to impaired channel trafficking and recycling along MTs.

Actin polymerization has also been reported to be an important determinant of cardiac ion channel trafficking, notably of Cx43 (51). Although we failed to visualize cortical F-actin because of the vast amount of sarcomeric actin in AMVMs, we found that actin disruption with lat-A led to reduced: i) ISO-stimulated mobilization of $Ca_V1.2$ from EEs (Figure 3H), and ii) augmentation of $Ca_V1.2$ channel expression in the PM, as indicated by super-resolution GSD imaging experiments (Figure 6C) and live-cell TIRF experiments on AAV9-$Ca_V\beta_{2a}$-paGFP transduced AMVMs (Figure 4E). Furthermore, lat-A significantly blunted adrenergic regulation of the channels assessed with whole cell patch clamp (Figure 5G-I and Table1). The degree of apparent channel insertions in response to ISO remained at a similar level to untreated cells suggesting that MTs, not actin, play the dominant role in channel delivery to the sarcolemma (Figure 4F). However, the pool of channels that was mobilized to the membrane in the presence of lat-A did not appear to belong to the EE pool, since colocalization between EEA1 and $Ca_V1.2$ channels was unchanged by ISO. In the Cx43 literature, it has been proposed that Cx43 cargo on its way to the sarcolemma from the golgi along MTs, pauses at actin 'rest-stops' before being handed off to additional MTs to complete its journey to the membrane (51, 52). It is possible that a similar 'rest stop' system exists for $Ca_V1.2$ channel delivery in cardiomyocytes and that lat-A mediated actin disruption and ISO-stimulation, releases this pool, allowing them to traffic to the sarcolemma along MTs. This intriguing hypothesis remains to be proven.

ISO-stimulation of AMVMs with a combined treatment with nocodazole and lat-A increased channel endocytosis as indicated by increased colocalization between EEs and $Ca_V1.2$ in Airyscan images (Figure 3J), and actually led to reduced channel expression in the sarcolemma in response to ISO (Figure 4E), while adrenergic regulation of the channel was completely eliminated (Figure 5J-L). On the basis of our functional patch clamp data, it is tempting to speculate that *βAR*-mediated regulation of $Ca_V1.2$ is heavily dependent

on this stimulated channel recycling pathway, however, ISO-stimulation is also known to induce endocytosis and subsequent fast, actin-dependent-recycling and resensitization of the receptors themselves (53-55). It is therefore possible that the lack of functional response is simply because of a lack of sarcolemmal *βAR* expression, as internalized receptors cannot recycle back to the membrane (56). To investigate this possibility, we bypassed the receptors and stimulated adenylyl cyclase directly with forskolin and studied the effect on channel dynamics in AAV9-$Ca_V\beta_{2a}$-paGFP transduced AMVMs using TIRF imaging (Supplemental Figure 4). Forskolin (1 μM) produced a similar increase in sarcolemmal $Ca_V\beta_{2a}$-paGFP expression (21.60 ± 3.72 %) as that observed with 100 nM ISO (27.95 ± 4.31 %). Treatment of AMVMs with cytoskeletal disruptors reduced the response (Figure S4B-E). These experiments do not totally rule out a direct *βAR* effect however, as although it is GRK-mediated phosphorylation of *βARs* that increases their affinity for β-arrestin, subsequent movement into clathrin-coated pits and endocytosis; PKA-mediated desensitization of *βARs* can occur with forskolin (57). However, in a 2-3 minute exposure to forskolin or ISO, previous studies have revealed that only 20-30% of the receptors would be rendered desensitized (58), and this cannot explain our observed abolition of *βAR*-regulation of I_{Ca} (Figure 4), suggesting that agonist-stimulated recycling of $Ca_V1.2$ is in fact a critical component of *βAR*-regulation of these channels.

After several decades of elusivity, the critical PKA phosphorylation site on the cardiac $Ca_V1.2$ channel complex was recently reported to be located on Rad, a member of the Rad/Rem/Rem2/Gem/Kir (RGK) family of monomeric GTP-binding proteins that interacts with the channel via the β-subunit (5). In a disinhibition process, Rad phosphorylation is said to cause dissociation from the channel complex releasing its inhibitory hold on the channel, and unveiling the larger I_{Ca} we recognize as *βAR*-regulation. A Rad-mediated $Ca_V1.2$ disinhibition hypothesis was also proposed several years earlier by Jonathan Satin's group when they reported that Rad knockout mice lost adrenergic regulation (6). So how does our *βAR*-stimulated recycling of $Ca_V1.2$ fit into this appealing model? We do not believe the two models are mutually exclusive but instead hypothesize that Rad inhibits $Ca_V1.2$ channel function by limiting its expression at the sarcolemma, an effect that is relieved when Rad is phosphorylated by PKA. Indeed, in addition to the ability of Rad to suppress channel activity by interfering with channel P_o, it has long been reported

that RGK-proteins, including Rad, also reduce I_{Ca} by limiting $Ca_V1.2$ expression at the sarcolemma (59-61). A previous study in PC12 cells reported that this effect of Rad on PM $Ca_V1.2$ channel expression relied on CaM-binding to Rad, such that mutation of the CaM binding site at L281G abrogated the inhibitory effect of Rad on I_{Ca} and increased detection of a HA-tagged $Ca_V1.2$ channel at the cell surface (59). In cells transfected with WT Rad, the cell surface transport of $Ca_V1.2$ was blocked. Our results in transduced AMVMs, and in tsA cells, illustrate that ISO-stimulates enhanced transport of channels to the cell surface. We speculate that this transport occurs when Rad is phosphorylated and dislodges from $Ca_V\beta$, releasing the channel complex and allowing more of it to traffic to the surface in a Rab4a and Rab11a dependent process. Indeed, that phosphorylation of Rad may be the 'upstream step' that has to occur before this recycling process is initiated, explaining why overexpression of CA-Rab4a does not raise the initial expression of $Ca_V1.2$ in the membrane in and of itself, but rather Rad phosphorylation must occur first. How PKA is anchored next to Rad on endosomes is another matter but may depend on the A-kinase anchoring protein D-AKAP2, which has been reported to regulate recycling of transferrin receptors via interactions with Rab4 and Rab11 (62). In line with that prediction, a human functional polymorphism in D-AKAP2 (I646V) is associated with reduced heart rate variability, indicative of a heart that cannot respond well to stressors (63). D-AKAP2 itself can be phosphorylated by PKA at residue 554 (62) and this may influence its localization. We briefly tested the hypothesis that ISO-stimulation of *βARs* would promote enhanced colocalization between D-AKAP2 and Rab11-positive endosomes finding an enhanced association (Figure S5). While this is admittedly, a correlative result, resolving these mechanistic details will make for an interesting future project.

Overall, our data indicate that there is an endosomal pool of intracellular $Ca_V1.2$ channels that is stimulated to recycle to the sarcolemma upon *βAR*-activation. Both Rab4a-mediated fast recycling pathways, and Rab11a-slow recycling pathways contribute to the response. Recycling channels insert into the sarcolemma by traveling along MTs likely anchored at the PM by BIN1. Cytoskeletal disruption creates traffic jams in the endosomal pathway and impedes the recycling response. Finally, electrophysiology data indicates that *βAR*-regulation of cardiac $Ca_V1.2$ channel function is abolished by treatments that interfere with this stimulated recycling pathway. Collectively, these results suggest that cardiomyocytes have an endosomal reservoir of $Ca_V1.2$ channels that is rapidly mobilized

to the sarcolemma in response to *βAR*-stimulation, and that this stimulated insertion is fundamentally required for *βAR*-regulation of these channels.

Materials and Methods

Detailed methods can be found in the SI Appendix. Briefly, AMVMs were enzymatically isolated using standard Langendorff technique as described previously (23, 64, 65). Fixed, immunostained AMVMs were imaged on a Zeiss Airyscan confocal microscope (as described in (66, 67)) or a Leica 3D-GSD-SR microscope to assess the distribution of $Ca_V1.2$ channels and various endosome populations (Airyscan only for the latter). Live cell TIRF imaging experiments of AAV9-$Ca_V\beta_{2a}$-paGFP transduced AMVMs or transiently transfected tsA-201 cells were performed on an Olympus IX-83 inverted microscope with a Cell-TIRF MITICO module. Live cell 4D-imaging of transduced AMVMs was performed at 37 °C on an Andor W-1 Spinning Disk confocal microscope. Rab mutant plasmids used for transient transfection of tsA-201 cells were gifts from Dr. Nipavan Chiamvimonvat (UC Davis, Davis, CA, USA) and Dr. Jose A. Esteban (*Centro de Biología Molecular 'Severo Ochoa' (CSIC-UAM)*, Madrid, Spain).

Acknowledgments

We wish to thank Dr. Luis Fernando Santana for the use of his GSD microscope, and for reading and commenting on this manuscript along with Dr. Manuel F. Navedo, and Dr. Maartje Westhoff.

Funding

This work was supported by NIH NIA grant R01AG063796 and AHA grant 15SDG25560035 to RED and an NIGMS grant R01GM127513 to EJD. Taylor Voelker and Heather Spooner were supported by a NIGMS-funded Pharmacology Training Program (T32GM099608).

Figures and Tables

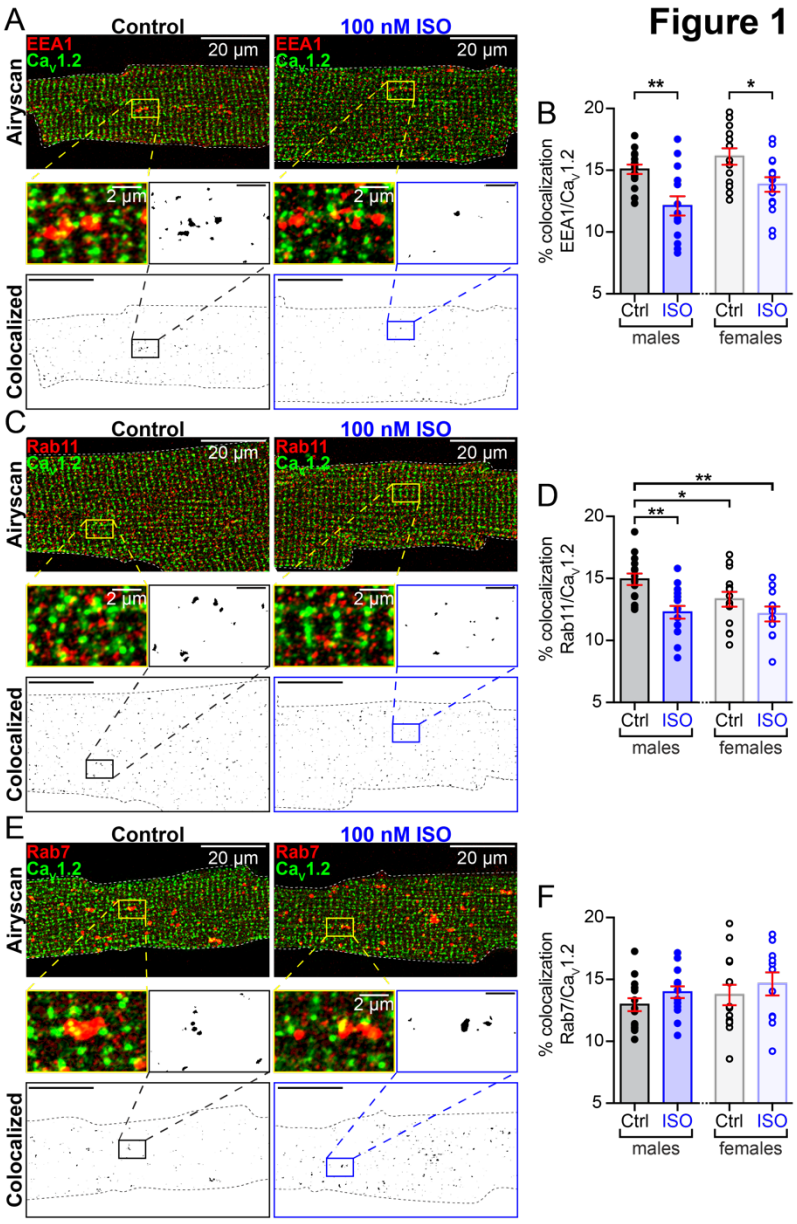

Figure 1. Internal pools of presynthesized Ca$_V$1.2 channels reside on endosomes. (*A*) Two-color Airyscan super-resolution images of control and 100 nM ISO-stimulated, AMVMs immunostained to examine distributions of Ca$_V$1.2 and EEA1 positive early endosomes. Binary colocalization maps (*bottom*) display pixels in which Ca$_V$1.2 and endosomal expression precisely overlapped. (*B*) Histograms showing % colocalization between EEA1 and Ca$_V$1.2 in male and female AMVMs, in control (male: $N = 3$, $n = 15$; female $N = 3$, $n = 13$) and ISO-stimulated conditions (male: $N = 3$, $n = 14$; female $N = 3$, $n = 15$). (*C*) Immunostaining of Ca$_V$1.2 and Rab11 positive recycling endosomes and (*D*)

accompanying histogram summarizing results from control (male: *N* = 4, *n* = 15; female *N* = 3, *n* = 14) and ISO conditions (male: *N* = 3, *n* = 15; female *N* = 3, *n* = 11). (*E*) Immunostaining of $Ca_V1.2$ and Rab7 positive LEs and lysosomes. (*F)* Histogram summarizing results from control (males: *N* = 3, *n* = 15, females: N = 3, n = 14) and ISO-stimulated AMVMs (males: *N* = 3, *n* = 15, females: N = 3, n = 11). Error bars indicate SEM. Two-way ANOVA **P < 0.01; *P < 0.05. Pictured are male AMVMs, for females see Figure S1.

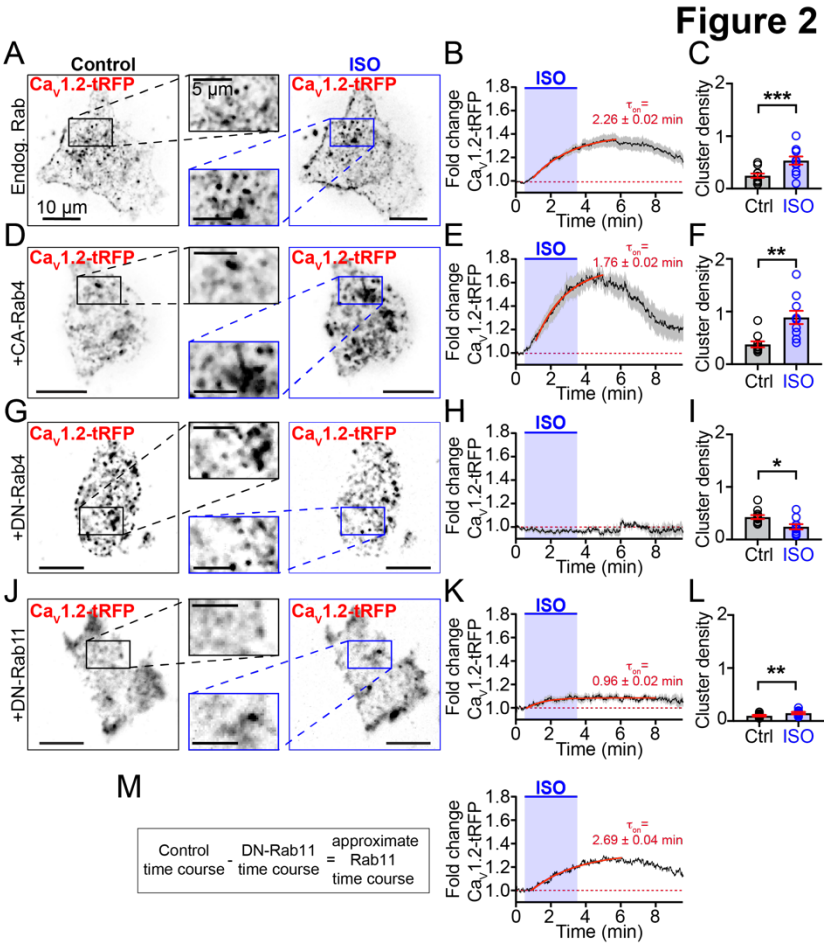

Figure 2. Rab4a and Rab11a regulate an ISO-stimulated boost in Ca$_V$1.2 recycling. (*A*) TIRF images of Ca$_V$1.2-tRFP distribution in the PM of tsA-201 cells before (*left*) and after 100 nM ISO (*right*; *n* = 18). (*B*) Time course and kinetics (solid red line) of the fold change in Ca$_V$1.2-tRFP intensity in the TIRF footprint before, during and after ISO stimulation. (*C*) Histogram summarizing Ca$_V$1.2 channel cluster density (number/µm^2) in the TIRF footprint in control and ISO stimulated conditions. (*D-F*) Same layout format in tsA-201 cells co-expressing constitutively active (GTP-locked) Rab4a (*n* = 10). (*G-I*) Same layout format in tsA-201 cells co-expressing dominant negative (GDP-locked) Rab4a (*n* = 12). (*J-L*) Same layout format in tsA-201 cells co-expressing dominant negative (GDP-locked) Rab11a (*n* = 8). (*M*) Calculation and resultant theoretical time-course and kinetics of Rab11a-dependent ISO-stimulated recycling.

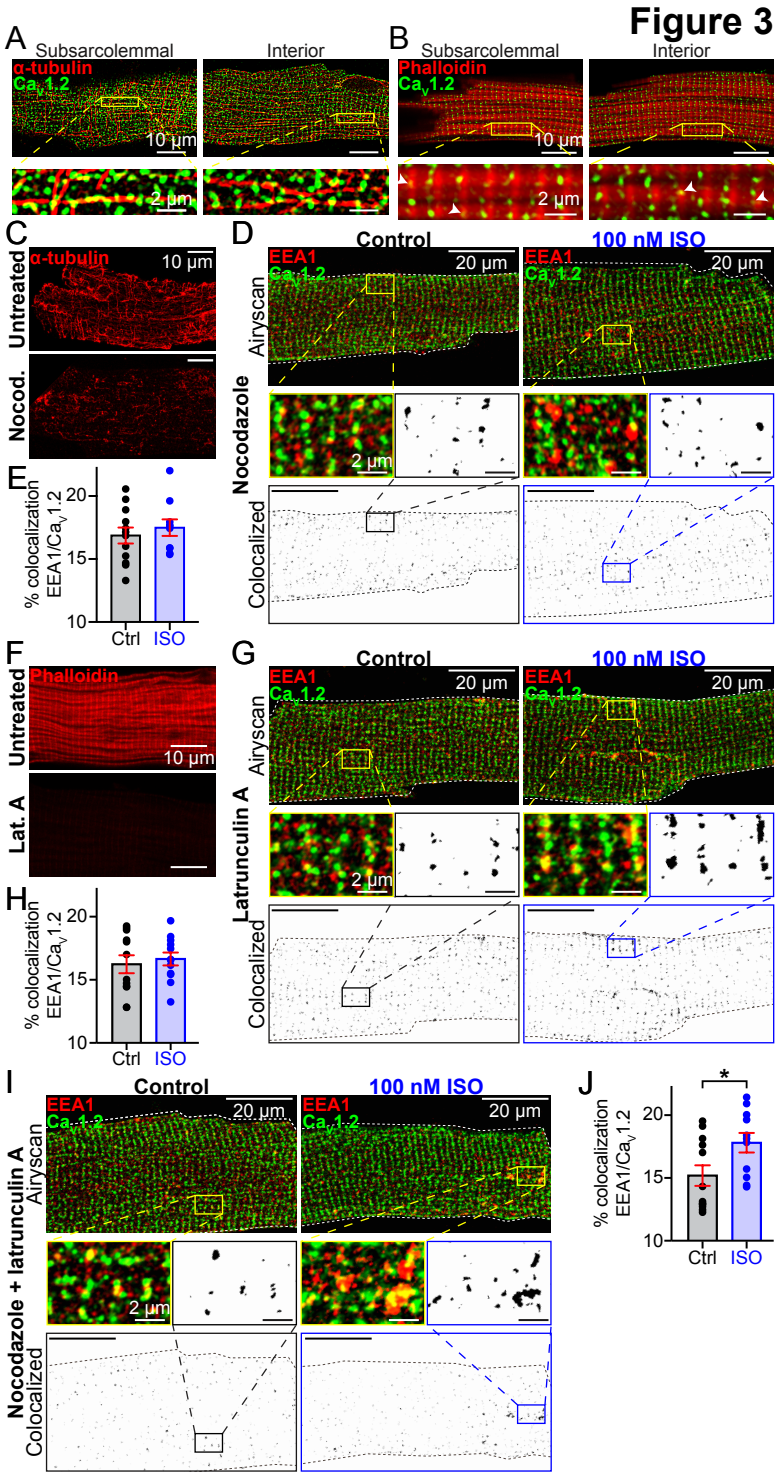

Figure 3. Actin and MT polymerization are essential for ISO-stimulated Ca$_V$1.2 recycling. Two-color Airyscan images of fixed AMVMs immunostained to examine the relative localization of Ca$_V$1.2 and (*A*) α-tubulin, or (*B*) phalloidin-stained actin. (*C*) shows the distribution of α-tubulin in untreated (*top*) and nocodazole-treated AMVMs (*bottom*).

(*D*) Airyscan images of $Ca_V1.2$ and EEA1 distribution in nocodazole-treated control (*N* = 3, *n* = 12; *left*) and ISO-stimulated (*N* = 3, *n* = 10; *right*) AMVMs. *Bottom*: binary colocalization maps display pixels in which $Ca_V1.2$ and EEA1 expression precisely overlapped. (*E*) Histogram summarizing % colocalization of EEA1 with $Ca_V1.2$ in nocodazole-treated cells. (*F*) Actin distribution in untreated (*top*) and latrunculin-A treated cells (*bottom*). (*G*) Airyscan images and binary colocalization maps of $Ca_V1.2$ and EEA1 distribution in latrunculin-A-treated control (*N* = 3, *n* = 12; *left*) and ISO-stimulated (*N* = 3, *n* = 12; *right*) AMVMs. (*H*) Histogram showing % colocalization of EEA1 with $Ca_V1.2$ in latrunculin-A-treated AMVMs. (*I*) Airyscan images and binary colocalization maps of AMVMs treated with both latrunculin-A and nocodazole under control (*N* = 3, *n* = 12) and ISO stimulated conditions (N = 3, n = 11), with accompanying summary histogram (*J*).

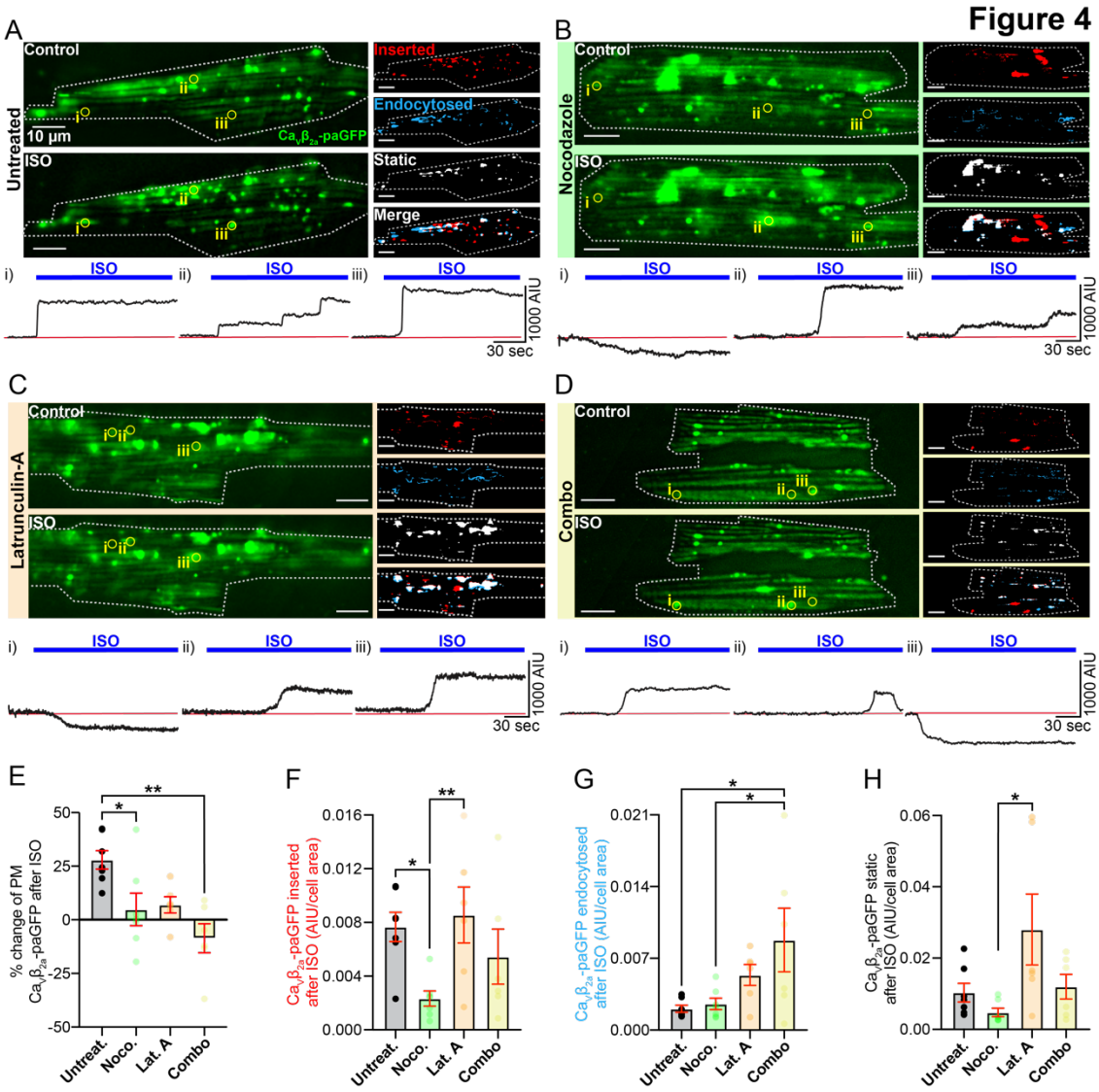

Figure 4. Dynamic imaging to unmask the mobile channel population. (*A*) TIRF images of GFP fluorescence emission from $Ca_v\beta_{2a}$-paGFP transduced AMVMs before (*top*) and after 100 nM ISO (*bottom*). Images illustrating inserted, endocytosed, static, and merged channel populations are shown to the right. *Bottom*: Time course of the changes in $Ca_v\beta_{2a}$-paGFP intensity in ROIs (i-iii) indicated by yellow circles on TIRF images. (N = 5, n = 7). Same format for cells pre-treated with (*B*) nocodazole (N = 5, n = 7), (*C*) latrunculin-A (N = 3, n = 6), or (*D*) both cytoskeleton disruptors (N = 3, n = 6). (*E-H*) Histograms summarizing statistics for these experiments.

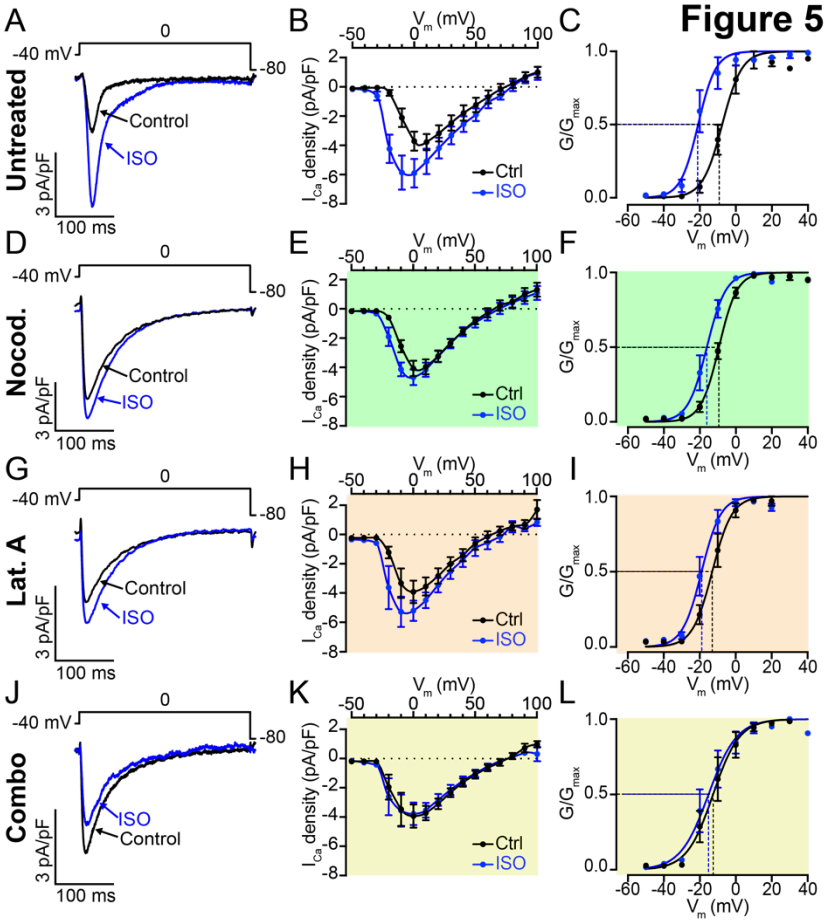

Figure 5. *β*AR mediated I_{Ca} enhancement is blunted by reducing dynamic channel insertion. (*A*) Whole cell currents elicited from a representative AMVM during a 300 ms depolarization step from -40 mV to 0 mV before (control: black) and during application of 100 nM ISO (blue). (*B*) I-V plot summarizing the results from *n* = 7 cells (from *N* = 7 animals) subjected to test potentials ranging from -50 mV to +100 mV. Currents were normalized to cell capacitance to generate current density. (*C*) Voltage-dependence of the normalized conductance (G/G_{max}) before and during ISO application, fit with Boltzmann functions. (*D-F*) show whole cell currents (*D*), I-V (*E*), and G/G_{max} plots (*F*) from AMVMs pre-treated for 2 hrs with 10 µM nocodazole (*N* = 4, *n* = 7). (*G-H*) show the same for cells treated with 5 µM lat-A (*N* = 5, *n* = 5). (*J-L*) show results from cells treated with a combination of both (*N* = 3, *n* = 6).

Figure 6

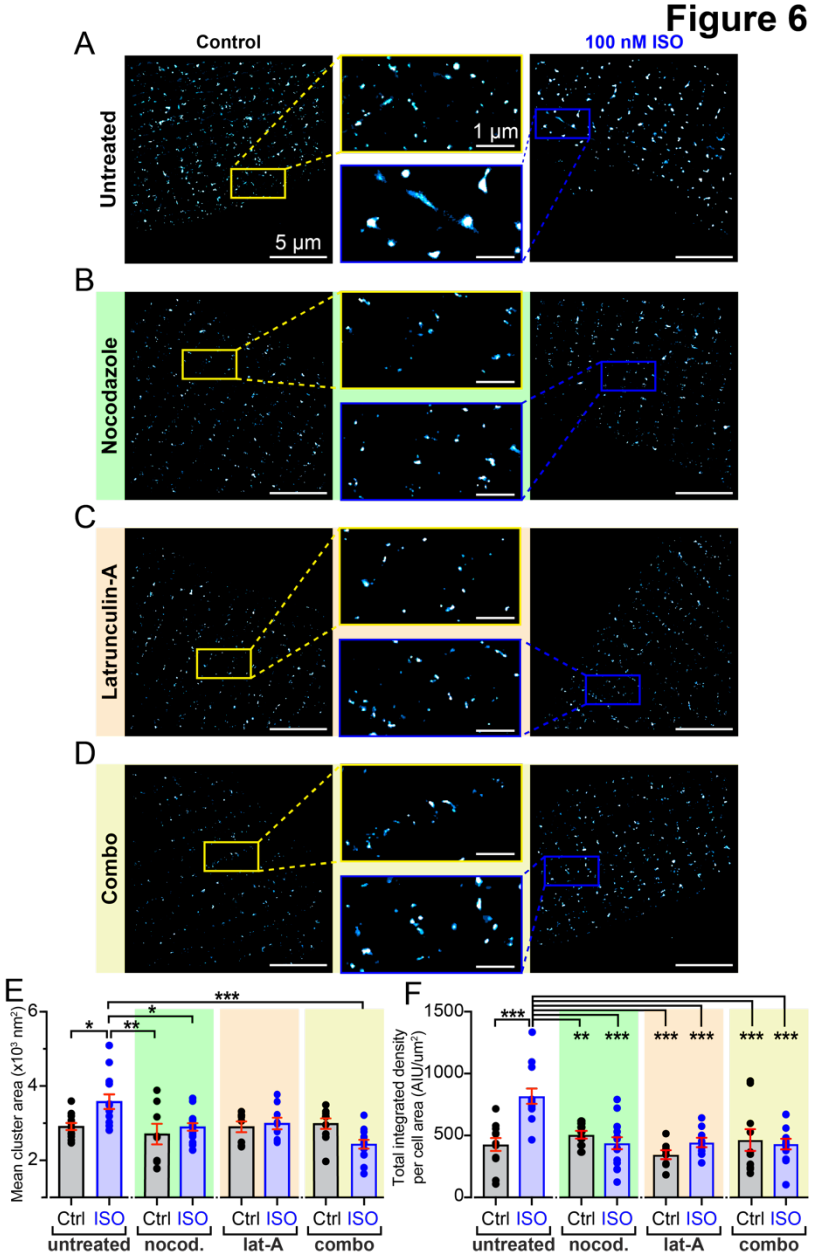

Figure 6. *β*AR-stimulated $Ca_V1.2$ super-clustering and enhanced sarcolemmal expression requires an intact MT cytoskeleton. Super-resolution GSD localization maps of control (*left*) and 100 nm ISO-stimulated (*right*), fixed, AMVMs immunostained to examine $Ca_V1.2$ channel distribution under (*A*) untreated (control: $N = 3$, $n = 13$; ISO: $N = 3$, $n = 13$), (*B*) nocodazole-treated (control: $N = 3$, $n = 8$; ISO: ($N = 3$, $n = 15$), (*C*) lat-A-treated (control: $N = 3$, $n = 8$; ISO: ($N = 3$, $n = 9$), and (*D*) combo-treated (control: $N = 2$, $n = 10$; ISO: ($N = 3$, $n = 13$) conditions. Maps were pseudocoloured 'cyan hot' and received a one-pixel median filter for display purposes. Yellow (*control*) and blue (*ISO*) boxes

indicate the location of the zoomed-in regions displayed in the center. (*E*) and (*F*), aligned dot plots showing mean $Ca_V1.2$ channel cluster areas and normalized total integrated density in each condition. Two-way ANOVA ***P<0.001, **P < 0.01, *P < 0.05.

Figure 7

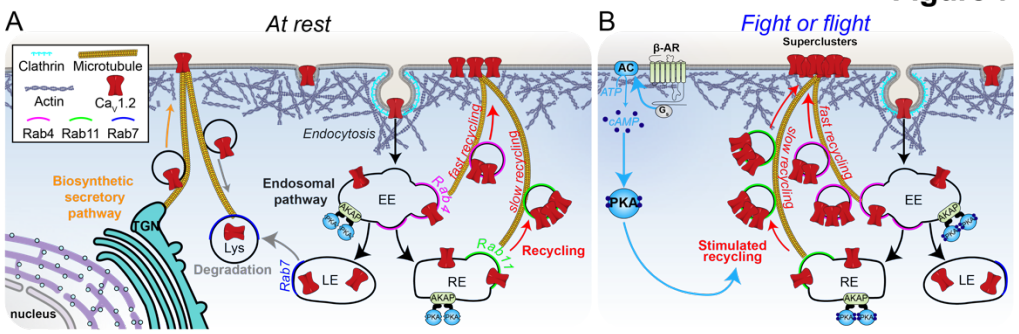

Figure 7. Our working model. *A*: $Ca_V1.2$ channels on the ventricular myocyte sarcolemma are subject to dynamic equilibrium under resting, unstimulated conditions. Channels synthesized in the Golgi are transferred to negative-end anchored MTs at the trans-Golgi network (TGN) and transported in motor-protein shuttled vesicles, to plus-end anchored BIN1 hubs at the membrane. Steady state channel expression is achieved as 'new' channel insertions are balanced by ongoing channel endocytosis and recycling through the endocytic pathway. *B:* Activation of *βAR*s by ISO or during fight or flight, leads to stimulated recycling of $Ca_V1.2$, from sub-sarcolemmal pools of Rab4a and Rab11a-positive endosomes. D-AKAP2 anchors PKA on endosomal membranes, future studies should investigate its role in *βAR*-stimulated channel recycling. Resultant 'on-demand' insertion of the endosomal reservoir of $Ca_V1.2$, leads to augmented $Ca_V1.2$ expression and super-clustering at the sarolemma, facilitates channel cooperativity, amplifies Ca^{2+}influx, and contributes to the enhanced I_{Ca} and inotropic response.

Table 1

	Fold-change in peak I_{Ca}	$V_{1/2}$ (mV)		Slope factor	
		Control	ISO	Control	ISO
Untreated	1.65 ± 0.19*	-7.57 ± 0.95	-20.90 ± 1.14****	5.45 ± 0.84	4.90 ± 1.06
Nocodazole	1.18 ± 0.08	-9.38 ± 0.44	-16.10 ± 0.84***	5.03 ± 0.41	5.27 ± 0.72
Latrunculin A	1.39 ± 0.13	-13.03 ± 0.87	-18.95 ± 0.97*	5.51 ± 0.76	5.33 ± 0.88
Noco + Lat.A	1.01 ± 0.11	-12.62 ± 1.40	-15.16 ± 1.53	7.32 ± 1.24	7.82 ± 1.36

References

1. S. Ringer, A further Contribution regarding the influence of the different Constituents of the Blood on the Contraction of the Heart. *J Physiol* **4**, 29-42 23 (1883).
2. H. Reuter, H. Scholz, The regulation of the calcium conductance of cardiac muscle by adrenaline. *J Physiol* **264**, 49-62 (1977).
3. D. T. Yue, S. Herzig, E. Marban, β-adrenergic stimulation of calcium channels occurs by potentiation of high-activity gating modes. *Proc Natl Acad Sci U S A* **87**, 753-757 (1990).
4. N. Sperelakis, J. A. Schneider, A metabolic control mechanism for calcium ion influx that may protect the ventricular myocardial cell. *The American journal of cardiology* **37**, 1079-1085 (1976).
5. G. Liu *et al.*, Mechanism of adrenergic $Ca_V1.2$ stimulation revealed by proximity proteomics. *Nature* **577**, 695-700 (2020).
6. J. R. Manning *et al.*, Rad GTPase deletion increases L-type calcium channel current leading to increased cardiac contraction. *J Am Heart Assoc* **2**, e000459 (2013).
7. X. Chen *et al.*, L-type Ca^{2+} channel density and regulation are altered in failing human ventricular myocytes and recover after support with mechanical assist devices. *Circ Res* **91**, 517-524 (2002).
8. J. He *et al.*, Reduction in density of transverse tubules and L-type Ca^{2+} channels in canine tachycardia-induced heart failure. *Cardiovascular research* **49**, 298-307 (2001).
9. I. R. Josephson, A. Guia, M. D. Stern, E. G. Lakatta, Alterations in properties of L-type Ca^{2+} channels in aging rat heart. *J Mol Cell Cardiol* **34**, 297-308 (2002).
10. T. T. Hong *et al.*, BIN1 is reduced and $Ca_V1.2$ trafficking is impaired in human failing cardiomyocytes. *Heart Rhythm* **9**, 812-820 (2012).
11. I. Pranke, A. Golec, A. Hinzpeter, A. Edelman, I. Sermet-Gaudelus, Emerging Therapeutic Approaches for Cystic Fibrosis. From Gene Editing to Personalized Medicine. *Front Pharmacol* **10**, 121 (2019).
12. A. J. Chien *et al.*, Roles of a membrane-localized beta subunit in the formation and targeting of functional L-type Ca^{2+} channels. *J Biol Chem* **270**, 30036-30044 (1995).
13. R. Conrad *et al.*, Rapid Turnover of the Cardiac L-Type $Ca_V1.2$ Channel by Endocytic Recycling Regulates Its Cell Surface Availability. *iScience* **7**, 1-15 (2018).
14. W. C. Claycomb *et al.*, HL-1 cells: a cardiac muscle cell line that contracts and retains phenotypic characteristics of the adult cardiomyocyte. *Proc Natl Acad Sci U S A* **95**, 2979-2984 (1998).
15. A. Wandinger-Ness, M. Zerial, Rab proteins and the compartmentalization of the endosomal system. *Cold Spring Harb Perspect Biol* **6**, a022616 (2014).
16. P. Buda *et al.*, Eukaryotic translation initiation factor 3 subunit e controls intracellular calcium homeostasis by regulation of $Ca_V1.2$ surface expression. *PLoS One* **8**, e64462 (2013).
17. H. Stenmark, Rab GTPases as coordinators of vesicle traffic. *Nat Rev Mol Cell Biol* **10**, 513-525 (2009).
18. E. Mizuno-Yamasaki, F. Rivera-Molina, P. Novick, GTPase networks in membrane traffic. *Annual review of biochemistry* **81**, 637-659 (2012).
19. F. R. Maxfield, T. E. McGraw, Endocytic recycling. *Nat Rev Mol Cell Biol* **5**, 121-132 (2004).
20. E. M. Green, C. F. Barrett, G. Bultynck, S. M. Shamah, R. E. Dolmetsch, The tumor suppressor eIF3e mediates calcium-dependent internalization of the L-type calcium channel $Ca_V1.2$. *Neuron* **55**, 615-632 (2007).

21. J. M. Best *et al.*, Small GTPase Rab11b regulates degradation of surface membrane L-type $Ca_V1.2$ channels. *Am J Physiol Cell Physiol* **300**, C1023-1033 (2011).
22. D. Ghosh *et al.*, Dynamic L-type $Ca_V1.2$ channel trafficking facilitates $Ca_V1.2$ clustering and cooperative gating. *Biochimica et biophysica acta* **1865**, 1341-1355 (2018).
23. D. W. Ito *et al.*, β-adrenergic-mediated dynamic augmentation of sarcolemmal $Ca_V1.2$ clustering and co-operativity in ventricular myocytes. *J Physiol* **597**, 2139-2162 (2019).
24. B. K. Atwood, J. Lopez, J. Wager-Miller, K. Mackie, A. Straiker, Expression of G protein-coupled receptors and related proteins in HEK293, AtT20, BV2, and N18 cell lines as revealed by microarray analysis. *BMC Genomics* **12**, 14 (2011).
25. M. Cormont *et al.*, Potential role of Rab4 in the regulation of subcellular localization of Glut4 in adipocytes. *Molecular and cellular biology* **16**, 6879-6886 (1996).
26. S. C. Calaghan, J. Y. Le Guennec, E. White, Cytoskeletal modulation of electrical and mechanical activity in cardiac myocytes. *Prog Biophys Mol Biol* **84**, 29-59 (2004).
27. I. Fujiwara, M. E. Zweifel, N. Courtemanche, T. D. Pollard, Latrunculin A Accelerates Actin Filament Depolymerization in Addition to Sequestering Actin Monomers. *Curr Biol* **28**, 3183-3192 e3182 (2018).
28. I. Spector, N. R. Shochet, Y. Kashman, A. Groweiss, Latrunculins: novel marine toxins that disrupt microfilament organization in cultured cells. *Science* **219**, 493-495 (1983).
29. W. E. Louch, K. A. Sheehan, B. M. Wolska, Methods in cardiomyocyte isolation, culture, and gene transfer. *J Mol Cell Cardiol* **51**, 288-298 (2011).
30. H. C. Hartzell, P. F. Mery, R. Fischmeister, G. Szabo, Sympathetic regulation of cardiac calcium current is due exclusively to cAMP-dependent phosphorylation. *Nature* **351**, 573-576 (1991).
31. J. Leroy *et al.*, Spatiotemporal dynamics of β-adrenergic cAMP signals and L-type Ca^{2+} channel regulation in adult rat ventricular myocytes: role of phosphodiesterases. *Circ Res* **102**, 1091-1100 (2008).
32. T. Hermosilla *et al.*, Prolonged AT1R activation induces $Ca_V1.2$ channel internalization in rat cardiomyocytes. *Sci Rep* **7**, 10131 (2017).
33. B. D. Grant, J. G. Donaldson, Pathways and mechanisms of endocytic recycling. *Nat Rev Mol Cell Biol* **10**, 597-608 (2009).
34. T. T. Hong *et al.*, BIN1 localizes the L-type calcium channel to cardiac T-tubules. *PLoS Biol* **8**, e1000312 (2010).
35. D. D. Hall *et al.*, Competition between alpha-actinin and Ca^{2+}-calmodulin controls surface retention of the L-type Ca^{2+} channel $Ca_V1.2$. *Neuron* **78**, 483-497 (2013).
36. P. Y. Tseng *et al.*, alpha-Actinin Promotes Surface Localization and Current Density of the Ca^{2+} Channel $Ca_V1.2$ by Binding to the IQ Region of the α_1 Subunit. *Biochemistry* **56**, 3669-3681 (2017).
37. G. H. Diering, R. L. Huganir, The AMPA Receptor Code of Synaptic Plasticity. *Neuron* **100**, 314-329 (2018).
38. A. M. Purkey, M. L. Dell'Acqua, Phosphorylation-Dependent Regulation of Ca^{2+}-Permeable AMPA Receptors During Hippocampal Synaptic Plasticity. *Front Synaptic Neurosci* **12**, 8 (2020).
39. P. I. Nedvetsky *et al.*, A Role of myosin Vb and Rab11-FIP2 in the aquaporin-2 shuttle. *Traffic* **8**, 110-123 (2007).
40. K. Fushimi, S. Sasaki, F. Marumo, Phosphorylation of serine 256 is required for cAMP-dependent regulatory exocytosis of the aquaporin-2 water channel. *J Biol Chem* **272**, 14800-14804 (1997).

41. L. Bao, K. Hadjiolova, W. A. Coetzee, M. J. Rindler, Endosomal K_{ATP} channels as a reservoir after myocardial ischemia: a role for SUR2 subunits. *Am J Physiol Heart Circ Physiol* **300**, H262-270 (2011).
42. M. Jiang, Y. Wang, G. N. Tseng, Adult Ventricular Myocytes Segregate KCNQ1 and KCNE1 to Keep the I_{Ks} Amplitude in Check Until When Larger IKs Is Needed. *Circ Arrhythm Electrophysiol* **10** (2017).
43. Y. Wang *et al.*, $[Ca^{2+}]_i$ elevation and oxidative stress induce KCNQ1 protein translocation from the cytosol to the cell surface and increase slow delayed rectifier (IKs) in cardiac myocytes. *J Biol Chem* **288**, 35358-35371 (2013).
44. G. Seebohm *et al.*, Regulation of endocytic recycling of KCNQ1/KCNE1 potassium channels. *Circ Res* **100**, 686-692 (2007).
45. D. Sato *et al.*, A stochastic model of ion channel cluster formation in the plasma membrane. *J Gen Physiol* 10.1085/jgp.201912327 (2019).
46. M. A. Caporizzo, C. Y. Chen, B. L. Prosser, Cardiac microtubules in health and heart disease. *Exp Biol Med (Maywood)* **244**, 1255-1272 (2019).
47. C. Y. Chen *et al.*, Suppression of detyrosinated microtubules improves cardiomyocyte function in human heart failure. *Nature medicine* **24**, 1225-1233 (2018).
48. B. M. Drum *et al.*, Oxidative stress decreases microtubule growth and stability in ventricular myocytes. *J Mol Cell Cardiol* **93**, 32-43 (2016).
49. H. Ouadid, B. Albat, J. Nargeot, Calcium currents in diseased human cardiac cells. *Journal of cardiovascular pharmacology* **25**, 282-291 (1995).
50. J. B. Strait, E. G. Lakatta, Aging-Associated Cardiovascular Changes and Their Relationship to Heart Failure. *Heart Failure Clinics* **8**, 143-+ (2012).
51. J. W. Smyth *et al.*, Actin cytoskeleton rest stops regulate anterograde traffic of connexin 43 vesicles to the plasma membrane. *Circ Res* **110**, 978-989 (2012).
52. S. S. Zhang, S. Hong, A. G. Kleber, L. P. Lee, R. M. Shaw, A micropatterning approach for imaging dynamic Cx43 trafficking to cell-cell borders. *FEBS Lett* **588**, 1439-1445 (2014).
53. A. C. Hanyaloglu, M. von Zastrow, Regulation of GPCRs by endocytic membrane trafficking and its potential implications. *Annual review of pharmacology and toxicology* **48**, 537-568 (2008).
54. R. Irannejad *et al.*, Conformational biosensors reveal GPCR signalling from endosomes. *Nature* **495**, 534-538 (2013).
55. G. A. Yudowski, M. A. Puthenveedu, A. G. Henry, M. von Zastrow, Cargo-mediated regulation of a rapid Rab4-dependent recycling pathway. *Mol Biol Cell* **20**, 2774-2784 (2009).
56. E. E. Millman *et al.*, Rapid recycling of beta-adrenergic receptors is dependent on the actin cytoskeleton and myosin Vb. *Traffic* **9**, 1958-1971 (2008).
57. J. Pitcher, M. J. Lohse, J. Codina, M. G. Caron, R. J. Lefkowitz, Desensitization of the isolated β_2-adrenergic receptor by β-adrenergic receptor kinase, cAMP-dependent protein kinase, and protein kinase C occurs via distinct molecular mechanisms. *Biochemistry* **31**, 3193-3197 (1992).
58. N. S. Roth, P. T. Campbell, M. G. Caron, R. J. Lefkowitz, M. J. Lohse, Comparative rates of desensitization of β-adrenergic receptors by the β-adrenergic receptor kinase and the cyclic AMP-dependent protein kinase. *Proc Natl Acad Sci U S A* **88**, 6201-6204 (1991).
59. P. Beguin *et al.*, Nuclear sequestration of beta-subunits by Rad and Rem is controlled by 14-3-3 and calmodulin and reveals a novel mechanism for Ca^{2+} channel regulation. *Journal of molecular biology* **355**, 34-46 (2006).

60. P. Beguin *et al.*, Regulation of Ca^{2+} channel expression at the cell surface by the small G-protein kir/Gem. *Nature* **411**, 701-706 (2001).
61. B. S. Finlin, S. M. Crump, J. Satin, D. A. Andres, Regulation of voltage-gated calcium channel activity by the Rem and Rad GTPases. *P Natl Acad Sci USA* **100**, 14469-14474 (2003).
62. C. T. Eggers, J. C. Schafer, J. R. Goldenring, S. S. Taylor, D-AKAP2 interacts with Rab4 and Rab11 through its RGS domains and regulates transferrin receptor recycling. *J Biol Chem* **284**, 32869-32880 (2009).
63. S. A. Neumann *et al.*, AKAP10 (I646V) functional polymorphism predicts heart rate and heart rate variability in apparently healthy, middle-aged European-Americans. *Psychophysiology* **46**, 466-472 (2009).
64. R. E. Dixon *et al.*, Graded Ca^{2+}/calmodulin-dependent coupling of voltage-gated $Ca_V1.2$ channels. *Elife* **4** (2015).
65. R. E. Dixon, C. Yuan, E. P. Cheng, M. F. Navedo, L. F. Santana, Ca^{2+} signaling amplification by oligomerization of L-type $Ca_V1.2$ channels. *Proc Natl Acad Sci U S A* **109**, 1749-1754 (2012).
66. S. A. Tiscione *et al.*, Disease-associated mutations in Niemann-Pick type C1 alter ER calcium signaling and neuronal plasticity. *J Cell Biol* **218**, 4141-4156 (2019).
67. O. Vivas, S. A. Tiscione, R. E. Dixon, D. S. Ory, E. J. Dickson, Niemann-Pick Type C Disease Reveals a Link between Lysosomal Cholesterol and $PtdIns(4,5)P_2$ That Regulates Neuronal Excitability. *Cell Rep* **27**, 2636-2648 e2634 (2019).